OFFICE OF NAVAL RESEARCH

Contract No. N00014-91-J-1409

Technical Report No. 151

Charge-Induced (1 × 3) Reconstruction of Au(110): Mechanistic Insights from Potentiodynamic Scanning Tunneling Microscopy in Alkali Iodide Electrolytes

by

Xiaoping Gao and Michael J. Weaver

Prepared for Publication

in

Surface Science

Department of Chemistry

Purdue University

West Lafayette, Indiana 47907-1393

February 1994

ABSTRACT

The nature of the local atomic-level and nanoscale structural changes associated with the charge-induced (1 × 3) reconstruction on Au(110) in alkali iodide electrolytes is explored by means of potentiodynamic scanning tunneling microscopy, i.e., with STM images obtained during electrode potential excursions where the surface transformations are triggered on a suitable (seconds) timescale. In potassium iodide electrolyte, the usual "three-missing-row" (1 × 3) structure is seen to be generated by single gold atomic-row segments shifting both across and along the $(1\bar{1}0)$ direction. In cesium iodide, however, at least two spatially as well as potentiodynamically resolvable steps were observed, involving the intermediate local formation of "one-missing-row" (1 × 3) domains by removal of one-third of the top layer gold rows onto nearby terrace regions. Domains having (1 × 2) symmetry were also discerned. A subsequent transformation into the final "three-missing-row" (1 × 3) structure is achieved by aggregation of the displaced monoatomic row segments. The mechanistic value of following atomic-level reconstruction processes by such coupled electrochemical-STM tactics is illustrated by these findings.

1. INTRODUCTION

Understanding the manner by which surface reconstruction occurs, as well as the equilibrium structures that form, is in most cases inadequately understood. Scanning tunneling microscopy (STM), however, is having a major impact on these issues, exploiting the remarkable ability of the technique to ascertain real-space local structures down to the atomic level[1]. In addition to metal surfaces in ultrahigh vacuum (uhv), high-quality atomic-level STM data is now obtainable at monocrystalline metal-solution interfaces[2]. Besides the intrinsic importance of such electrochemical interfaces, an additional external means of structural (and kinetic) control is available in the form of the electrode potential. A number of recent studies using in-situ STM[3-10] and also X-ray scattering (SXRS)[11-14] have shown in remarkable detail the nature of the reconstructions that can be formed and removed at low-index gold surfaces in aqueous media in the presence of negative and positive electronic charges, respectively, induced by altering the electrode potential. Related phenomena have also been observed for some stepped gold surfaces[15]. Significantly, this sensitivity of the surface metal structure to the electrode potential can yield detailed insight into the surface morphological changes attending the formation and removal of the reconstruction. A particularly useful tactic, which has been dubbed "potentiodynamic" STM, involves acquiring sequences of images during (or immediately following) potential sweeps and steps[9,10]. This can enable the extraction of real-time/-space information on the reconstruction mechanisms.

A surface which has attracted particular attention with regard to surface reconstruction in electrochemical[5,7,13,15] as well as uhv environments is Au(110) (see refs. 16 and 17 for an introduction to the extensive uhv literature). While the clean surface in uhv forms a stable (1 × 2) "missing-row" phase, (1 × 3) and even higher-order reconstructions are produced in the presence

of alkali-metal adsorption[17-19]. A similar (1 × 3) "three-missing-row" ("facetted") reconstruction[20,21] has been observed for Au(110) at negative charges in aqueous alkali halide electrolytes[13], whereas predominantly (1 × 2) domains are formed in weakly (or non-) adsorbing aqueous media[5,7,15b].

We report here potentiodynamic STM data obtained on Au(110) in alkali iodide electrolytes, primarily under cyclic voltammetric conditions. The presence of adsorbed iodide yields a uniform (1 × 1) (i.e., reconstructed) phase at positive electronic charge densities. The addition of negative charge (i.e., sweeping the electrode potential more negative) induces a phase transition yielding a (1 × 3) structure. In cesium iodide electrolyte, however, the transition is seen to occur in several resolvable steps. The local structural changes associated with these steps, which are readily discernable by STM, provide mechanistic insight which may have more general implications.

2. EXPERIMENTAL

The experimental details for in-situ STM are described elsewhere[2,7]. The microscope is a Nanoscope II (Digital Instruments) with a bipotentiostat for electrochemical STM. The Au(110) single crystal (hemisphere, 5 mm diameter) was flame annealed, cooled partly in air and then in ultrapure water, and transferred immediately to the STM cell. The STM tip was an electrochemically etched tungsten wire. Most STM images were obtained in the "constant-current" mode, and are shown here in unfiltered form. The voltammetric data were obtained in a conventional (nitrogen-purged) electrochemical cell. While comparable results could also be observed in the STM cell, the voltammetric features at negative potentials tend to be masked by faradaic currents for oxygen reduction. All electrode potentials are reported here versus the saturated calomel electrode (SCE).

3. RESULTS AND DISCUSSION

Figure 1 shows a pair of typical cyclic voltammograms obtained for ordered Au(110) under conditions that are similar to those employed for the present STM results. The upper voltammogram was obtained at 10 mV s^{-1} in 50 mM $KClO_4$ + 5 mM KI. As detailed elsewhere[22], the cation-sensitive voltammetric features observed over the electrode potential range shown, −0.25 to −1.2 V vs. SCE, are indicative of marked potential-induced alterations in the interfacial structure and composition. (Additional, cation-insensitive, transitions are also evident at higher potentials[22].) The current spikes marked c/c′ and surrounding features arise from the reversible removal/formation of ordered coadsorbed alkali iodide adlayers[22].

Of particular interest here are the voltammetric peaks labelled b/b′ in Fig. 1. As discerned from the STM data and by analogy with related systems such as Au(100)-I^-[10,23], these features are associated with the removal and formation, respectively, of Au(110) reconstruction. Figures 2A and B show two images obtained during a potentiodynamic STM sequence under conditions similar to Fig. 1A, for Au(110) in 10 mM KI at 10 mV s^{-1} from −0.45 to −0.85 V and return. The first image was obtained while the potential was swept between −0.6 to −0.8 V. Since the image as shown was obtained by downward rastering (consuming 20 s), the y-axis can be considered to be a (downward-pointing) linear scale of electrode potential and time.

Close inspection of the STM data (Fig. 2A) in conjunction with the corresponding voltammetric segment in Fig. 1A, reveals that the reconstruction is initially discernable about a quarter of the way down the image, at about −0.65 V, corresponding to the foot of the voltammetric feature marked b′. The reconstruction appears as arrays of bright strings parallel to the $(1\bar{1}0)$ direction, initially spreading out preferentially from the semi-circular terrace

edges evident in Fig. 1A, thereby forming extended kinks. These bright strings each consist of individual gold atomic rows added to the initially (1 × 1) terrace. The source of these atoms appears to be partly the highest (top) terrace, and also the adjacent lower terrace as evidenced from the occurrence of nearby missing rows. By the time the twin voltammetric peaks labelled b′ in Fig. 1A are reached, at −0.7 to −0.75 V (corresponding to one-half to three-quarters down Fig. 2A), at least local areas of densely packed strings are seen yielding mostly (1 × 3) patterns. In addition to these "bright" added-row regions, nearby areas containing periodic missing rows are evident from the STM z-corrugations, which also approximate (1 × 3) symmetry.

Figure 2B shows the next STM image, now obtained by rastering the tip back upwards while the potential was swept from −0.8 to −0.85 V and back to −0.7 V. Most of the imaged region, encompassing the same five terrace domains as in Fig. 2B, is now seen to have been transformed into largely uniform (1 × 3) regions, with z-corrugations consistent with the usual three-missing-row structure (vide infra). Subsequent STM images show that the (1 × 3) structure reverts clearly to the (1 × 1) arrangement during traversal of the voltammetric peak b.

Substantially different behavior, however, was observed in similar potentiodynamic STM images gathered for Au(111) in CsI electrolytes. Figure 3A–F displays such an image sequence obtained in 10 mM CsI, during 5 mV s^{-1} potential excursion from −0.5 to −0.95 V and return, arranged so to span the region where the voltammetric features b_1, b_2/b_1', b_2', b_3' are located (Fig. 1B). The first image (A), obtained while holding the potential at −0.5 V, shows a large (ca 80 × 20 nm) terrace, surrounded by several lower terraces. Although not discernable at the magnification used here, a uniform (1 × 1) domain is present, the $(1\bar{1}0)$ direction running diagonally from the lower right-hand to the top left-hand corner of the image. The next, upward-rastered, image (Fig. 3B), was acquired

while the potential was swept negative from -0.55 to -0.65 V at 5 mV s^{-1}.

Comparison between Fig. 3A and B shows that formed in the latter are arrays of small (ca 4 by 10 Å) holes, about 1.5 Å (i.e. one-atom) deep, populated throughout the terraces. These features appear similar to those observed in the early stage of the K-induced reconstruction of Cu(110) in uhv[24]. Towards the top of Fig 3B (i.e., approaching -0.65 V, at the foot of wave b_1' in Fig. 1B), and especially close to the terrace edges, a (1 × 3) reconstruction becomes evident. The next, downward-rastered, image (Fig. 3C), was obtained during the ensuing potential-sweep segment from -0.65 to -0.75 V. This potential sector corresponds to the voltammetric region between b_1' and b_2' at the 5 mV s^{-1} sweep-rate employed. Evident in Fig. 3C is a uniform (1 × 3) reconstruction pattern throughout the terraces, of the type seen to be initiated in the upper region of the preceding image (A).

Detailed examination of the reconstruction profile from the STM images, however, indicates that the nature of this (1 × 3) reconstruction is quite different from the type seen to be generated in the KI electrolyte (Fig. 2). The latter exhibits a symmetric "v-shaped" z x profile across the $(1\bar{1}0)$ direction, with a ca 2 Å corrugation between the monoatomic rails, corresponding to the common "three-missing-row" structure (vide infra). The (1 × 3) reconstruction seen in Fig. 3C, however, consists of *pairs* of adjacent (110) monoatomic "rails", each separated by a single missing row. This is shown more clearly in the "blow-up" image of a portion of Fig. 3C, shown in Fig. 4A. A typical z-x corrugation profile (along the straight line marked on Fig. 4A) is shown in the top left-hand segment of Fig. 5. The matching ball model is shown on the top right-hand side: this has been termed the "one-missing-row" (1 × 3) structure[20,21]. An atomic-resolution image showing this paired-row arrangement is given in Fig. 4B. While (1 × 1) regions dominate the center region, (1 × 3) segments are seen towards the

right-hand side. Such images confirm that the top-layer ordered rows consist of gold, rather than cesium and/or iodide, based on the measured interatomic distance (2.9 ± 0.1 Å).

This alternate (1 × 3) structure is rarely seen, although it has been observed by STM to form upon during higher K coverages on Cu(110) in uhv[24]. The one-missing-row structure is nonetheless quite stable in the present case, remaining prevalent when the potential is held within the range ca −0.65 to −0.75 V for at least 30 min. Interestingly, the fate of the missing one-third row atoms is clearly evident in Fig. 3C: they are shifted so to form single- and double-atomic string segments on top of the (1 × 3) lattice; appearing as bright rows in Fig. 3C. (The bright strings are largely absent close to the terrace edges. The excess atoms have been incorporated into the steps, as indicated clearly from the increased size of the largest terrace evident upon comparing Fig. 3A and C.)

Further structural changes are seen in the next, upward-rastered, image (Fig. 3D), corresponding to a potential sweep from −0.75 V to −0.85 V (i.e. straddling the voltammetric peak b'_2 and an additional "satellite" peak, b'_3, appearing at slightly more negative potentials). A markedly increased density of bright (adlayer) strings is evident, along with the formation of surrounding (1 × 2) corrugated regions. A higher-magnification reproduction of a portion of Fig. 3D showing the (1 × 2) regions is displayed in Fig. 4C. A z-x profile obtained along the line marked in Fig. 4C is shown in Fig. 5 (left-middle), shown alongside the ball model for the (1 × 2) "missing-row" structure. The close relationship between the (1 × 2) and (1 × 3) one-missing-row structures is evident in Fig. 5; production of the former provides an additional source of the "added-row" atomic strings.

This conversion process continues at higher potentials, at −0.85 to −0.95

V, until a nearly uniform array of the adlayer strings is formed (Fig. 3E), now exhibiting (1 × 3) symmetry of the "three-missing-row" type. This final reconstructed form is similar to that produced in KI electrolytes (Fig. 2). A typical z–x plot culled from Fig. 3E is included in Fig. 5 (lower), alongside the corresponding ball-model structure. Interestingly, the magnitude of the ordered z–x STM corrugation for this structure, as well as the other two models shown in Fig. 5 matches well with the predicted ball models, especially when the anticipated occurrence of surface relaxation[25] is considered. A high-quality atomic-resolution image of the symmetrical (1 × 3) structure is given in Fig. 4D. This example was obtained in 0.1 M $HClO_4$ (at −0.4 V); images exhibiting such atomic detail are very difficult to obtain at the larger negative electrode potential required to trigger reconstruction in the iodide electrolytes. Evident in Fig. 4D is indeed an x–y surface relaxation whereby the gold rows adjacent to the center top strings are displaced outwards, by 0.6(± 0.2) Å.

The last image shown in this potentiodynamic STM sequence, Fig. 3F, was obtained by downward rastering while the potential was swept from −0.6 to −0.5 V. The early (i.e., upper) portion of this image shows the presence of the one-missing-row (1 × 3) structure giving way to an unreconstructed smooth terrace once the voltammetric peak b_1 (Fig. 1B) has been traversed. Comparison of the first and last images in this sequence (Fig. 3A and F, respectively), illustrates that the sequential potential-induced formation and removal of the reconstruction incurs substantial changes in the terrace-edge morphology. This confirms the occurrence of substantial nanoscale mass transport. Also note the presence of "island strands" of gold seen atop the large terrace in Fig. 3F; these, however, are dissipated with 1–2 min.

The present findings therefore demonstrate that the formation of the (1 × 3) reconstruction in alkali halide media is not only sensitive to the nature of

the cation, but also that spatially as well as potentiodynamically distinct steps can be resolved in the Cs^+ electrolyte. This cation sensitivity is undoubtedly connected with the specific adsorption of cesium known to occur on Au(110) under these conditions[22]. One therefore might be tempted to draw a close analogy with the alkali metal-induced (1 × 3) reconstruction seen for (110) surfaces in uhv[17-19]. Aside from the presence of iodide, however, the electrochemical system differs from its uhv counterpart in that the negative charge triggering the reconstruction for the former is inserted electronically (from the potentiostat), the cesium ions acting as a double-layer countercharge. (This charging is evident directly from the *nonfaradaic* voltammetric response which constitutes the b/b′ peaks in Fig. 1.) For the uhv system, the alkali metal dosed onto the surface acts itself as the electron source.

Most importantly, the ability to control and vary sensitively the surface electronic charge during sequential STM imaging in the electrochemical system reveals significant new detail concerning the real-space transformations leading to the final (1 × 3) reconstruction. The mechanism followed to form the three-missing-row structure, at least for the cesium electrolyte, does not involve merely short-range row shifting as might be expected given that this structure contains the same net gold atomic density as the (1 × 1) surface. Rather, the route chosen by the system is distinctly more elegant, involving an intermediate production of the "one-missing-row" (1 × 3) structure, the displaced rows (one-third of the original top layer atoms) themselves forming nearby (1 × 3) segments that eventually envelope the entire surface, yielding the familiar "three-missing-row" pattern.

Acknowledgments

We thank Greg Edens for obtaining the cyclic voltammograms and Antoinette Hamelin for preparing the Au(110) crystal. This work is supported by the Office of Naval Research and the National Science Foundation.

References

1) J. Wintterlin and R.J. Behm, in "Scanning Tunneling Microscopy I", Springer Series in Surface Sciences, Vol. 20, H-J. Güntherodt and R. Wiesendanger, eds., Springer-Verlag, Berlin, 1992, Chapter 4.

2) M.J. Weaver and X. Gao, Ann. Rev. Phys. Chem., 44 (1993), 459.

3) (a) X. Gao, A. Hamelin, and M.J. Weaver, Phys. Rev. Lett., 67 (1991), 618; (b) X. Gao, A. Hamelin, and M.J. Weaver, Phys. Rev. B, 46 (1992), 7096; (c) X. Gao and M.J. Weaver, Ber. Bunsenges Phys. Chem., 97 (1993), 507.

4) X. Gao, A. Hamelin, and M.J. Weaver, J. Chem. Phys., 95 (1991), 6993.

5) X. Gao, A. Hamelin, and M.J. Weaver, Phys. Rev. B., 44 (1991), 10983.

6) (a) N.J. Tao and S.M. Lindsay, J. Appl. Phys., 70 (1991), 5141; (b) N.J. Tao and S.M. Lindsay, Surf. Sci., 274 (1992), L546.

7) O.M. Magnussen, J. Wiechers, and R.J. Behm, Surf. Sci., 289 (1993), 139.

8) O.M. Magnussen, J. Hotlos, R.J. Behm, N. Batina, and D.M. Kolb, Surf. Sci., 296 (1993), 310.

9) X. Gao, G.J. Edens, A. Hamelin, and M.J. Weaver, Surf. Sci., 296 (1993), 333.

10) X. Gao and M.J. Weaver, J. Phys. Chem., 97 (1993), 8685

11) B.M. Ocko, J. Wang, A. Davenport, and H. Isaacs, Phys. Rev. Lett., 65 (1990), 1466.

12) J. Wang, B.M. Ocko, A. Davenport, and H. Isaacs, Phys. Rev. B., 46 (1992), 10321.

13) B.M. Ocko, G. Helgensen, B. Schardt, J. Wang, and A. Hamelin, Phys. Rev. Lett., 69 (1992), 3350.

14) I.M. Tidswell, N.M. Markovic, C.A. Lucas, and P.N. Ross, Phys. Rev. B, 47 (1993), 16542.

15) (a) X. Gao, A. Hamelin, and M.J. Weaver, Surf. Sci., 274 (1992), L582; (b) X. Gao, G.J. Edens, A. Hamelin, and M.J. Weaver, Surf. Sci., submitted.

16) T. Gritsch, D. Coulman, R.J. Behm, and G. Ertl, Surf. Sci., 257 (1991), 297.

17) D.K. Flynn-Sanders, H.D. Jamison, J.V. Barth, J. Wintterlin, P.A. Thiel, G. Ertl, and R.J. Behm, Surf. Sci., 253 (1991), 270.

18) R.J. Behm, D.K. Flynn, K.D. Jamison, G. Ertl, and P.A. Thiel, Phys. Rev. B, 36 (1987), 9267.

19) P. Häberle, P. Fenter, and T. Gustafsson, Phys. Rev. B, 39 (1989), 5810.

20) F. Masson and J.W. Rabalais, Surf. Sci., 253 (1991), 258.

21) P.A. Thiel and P.J. Estrup, in "CRC Handbook of Surface Imaging and Visualization", A.T. Hubbard, ed., CRC Press, in press.

22) X. Gao and M.J. Weaver, J. Phys. Chem., submitted.

23) X. Gao, G.J. Edens, F-C. Liu, and M.J. Weaver, in preparation.

24) R. Schuster, J.V. Barth, G. Ertl, and R.J. Behm, Surf. Sci., 247 (1991), L229.

25) I.K. Robinson, P.J. Eng, C. Romainczyk, and K. Kern, Phys. Rev. B, 47 (1993), 10700.

FIGURE CAPTIONS

Figure 1

Typical cyclic voltammograms, showing region where surface reconstruction occurs, for Au(110) in

A) 50 mM $KClO_4$ + 5 mM KI (at 10 mV s^{-1});

B) 50 mM $CsClO_4$ + 5 mM CsI (at 5 mV s^{-1}).

Figure 2

Large-scale potentiodynamic STM images for Au(110) in 10 mM KI obtained during initially negative-going 10 mV s^{-1} potential sweep. A) Downward-rastered image, during sweep from -0.6 to -0.8 V vs. SCE; B) Upward-rastered image, from -0.8 to -0.85 V and return to -0.7 V.

Figure 3

Sequence of large-scale potentiodynamic STM images for Au(110) in 10 mM CsI obtained during 5 mV s^{-1} potential sweep from -0.45 V to -0.85 V and return. Electrode potential, tip-rastering conditions as follows: A) -0.5 V (fixed potential); B) -0.55 to -0.65 V, upward raster; C) -0.65 to -0.75 V, downward raster; D) -0.75 to -0.85 V, upward raster; E) -0.85 to -0.95 V, downward raster; F) -0.6 to -0.5 V, downward raster.

Figure 4

Higher-magnification STM images showing various atomic-level details of Au(110) reconstruction patterns. A) "Blow-up" of upper left-hand region of Fig. 3C, showing one-missing-row structural pattern; B) Height-shaded atomic-resolution image, showing one-missing-row structure (right-hand region) and adjacent (1 × 1) domains; C) "Blow-up" of lower-portion of Fig. 3D, showing (1 × 2) missing row regions; D) Detailed atomic-resolution image (constant-height mode) for Au(110) in 0.1 M $HClO_4$ at -0.4 V, showing relaxed three-missing-row (1 × 3) structure. Straight-line segments drawn on A and C denote directions used to generate z-x profile plots shown in Fig. 5.

Figure 5

Z-corrugation profiles (z-x plots) along direction periodic to $(1\bar{1}0)$, obtained from STM images in Fig. 4 in comparison with schematic ball models for (1 × 3) one-missing-row, (1 × 2) missing row, and (1 × 3) three-missing-row reconstructions observed for Au(110). Top two z-x profiles refer to line segments drawn in Figs. 4A and C, respectively.

NOTE TO PRINTER:

IF POSSIBLE, PLEASE PLACE THE FIGURE 3 AND FIGURE 4 SET OF SIX AND FOUR IMAGES, RESPECTIVELY, AS "CLUSTERS" -

FIGURE 3		*FIGURE 4*	
A	*B*	*A*	*B*
C	*D*	*C*	*D*
E	*F*		

THANKS!

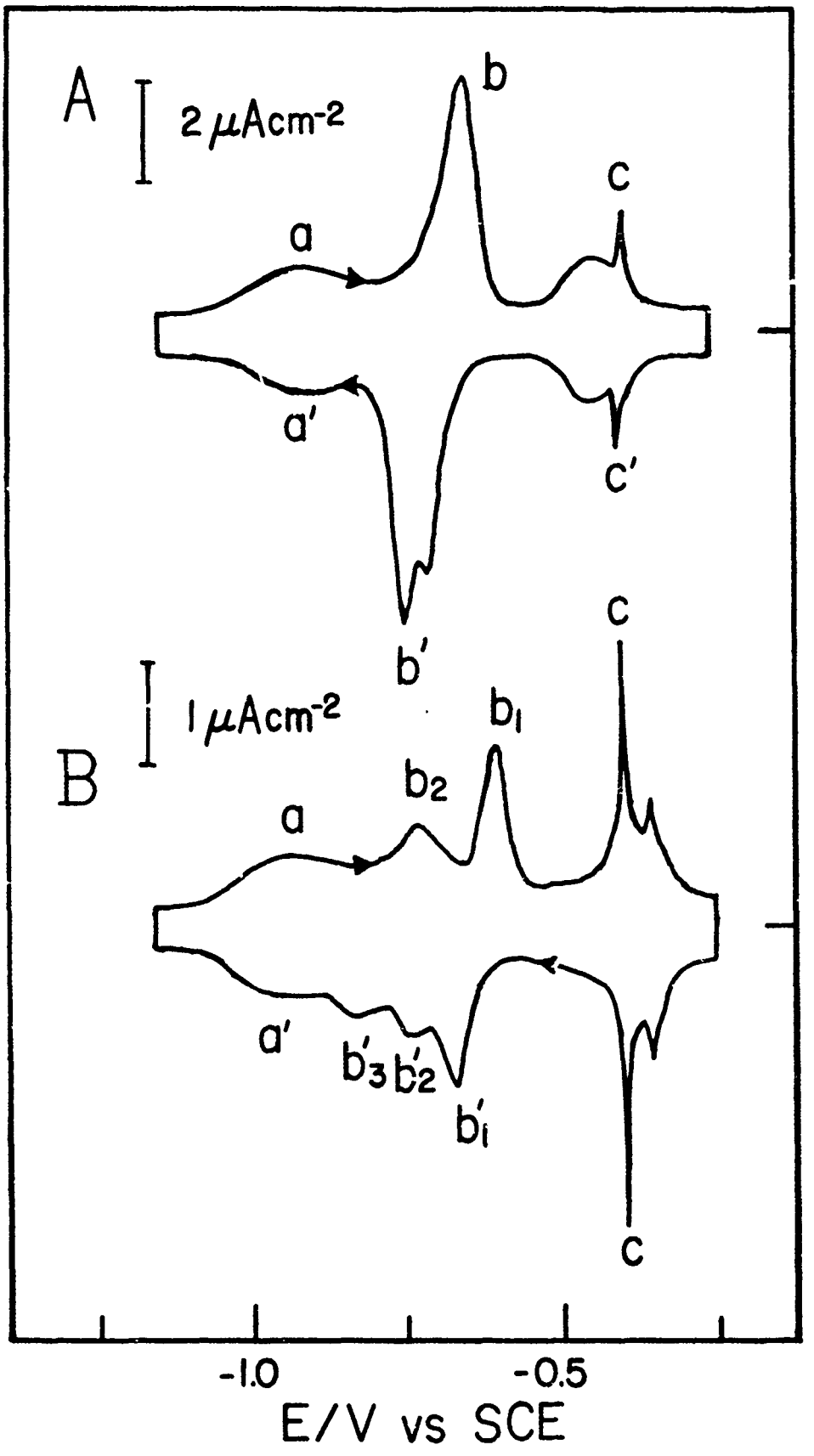

FIG 1

B

A

FIG 2

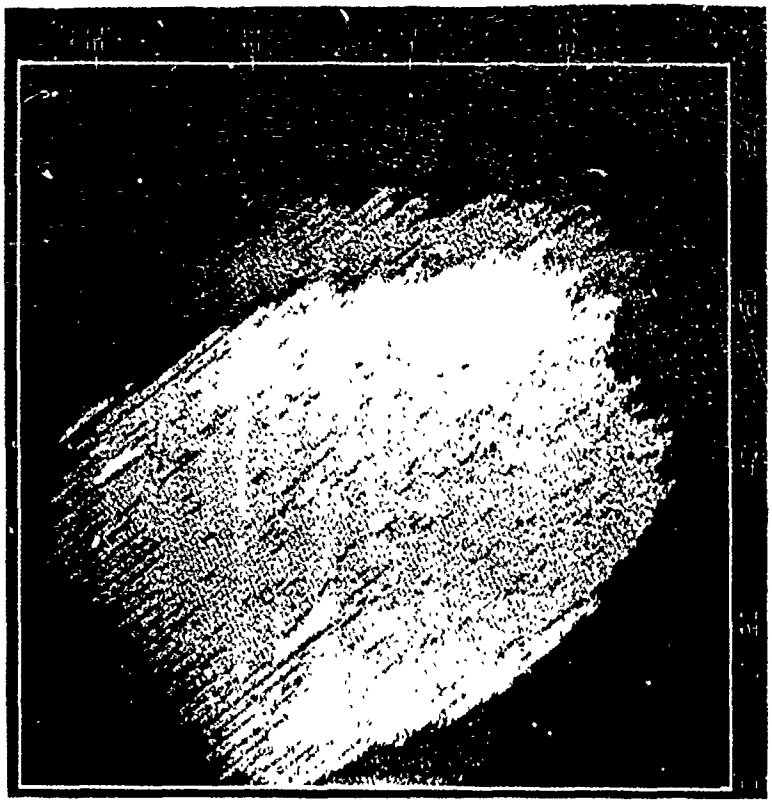

B

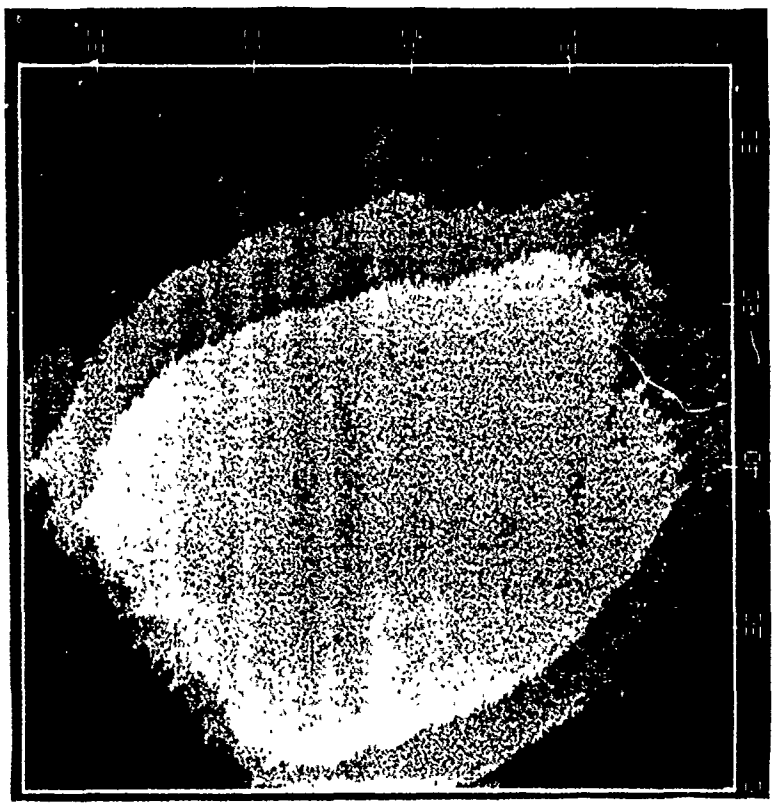

A

FIG 3

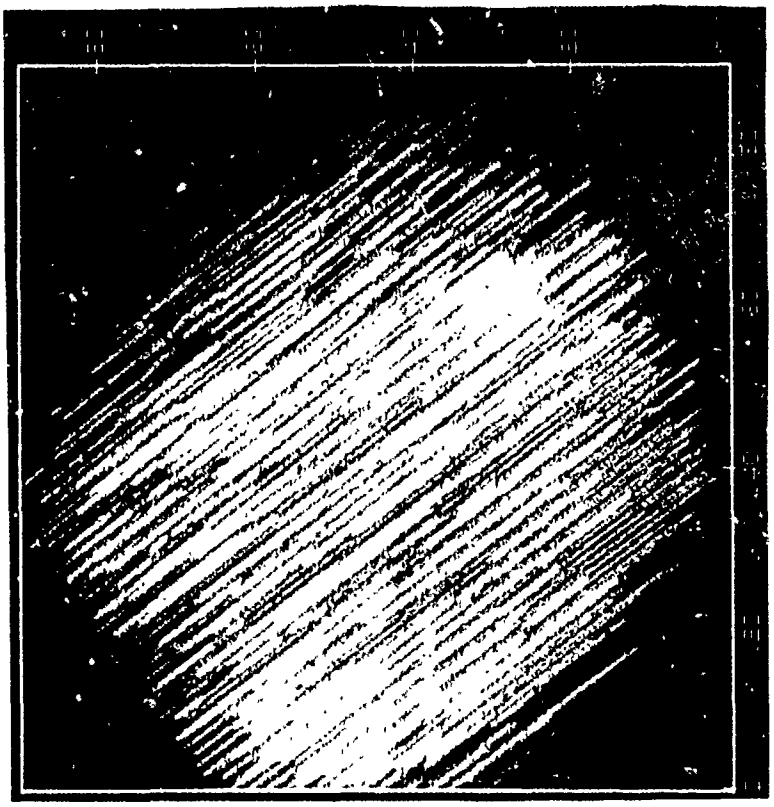

A

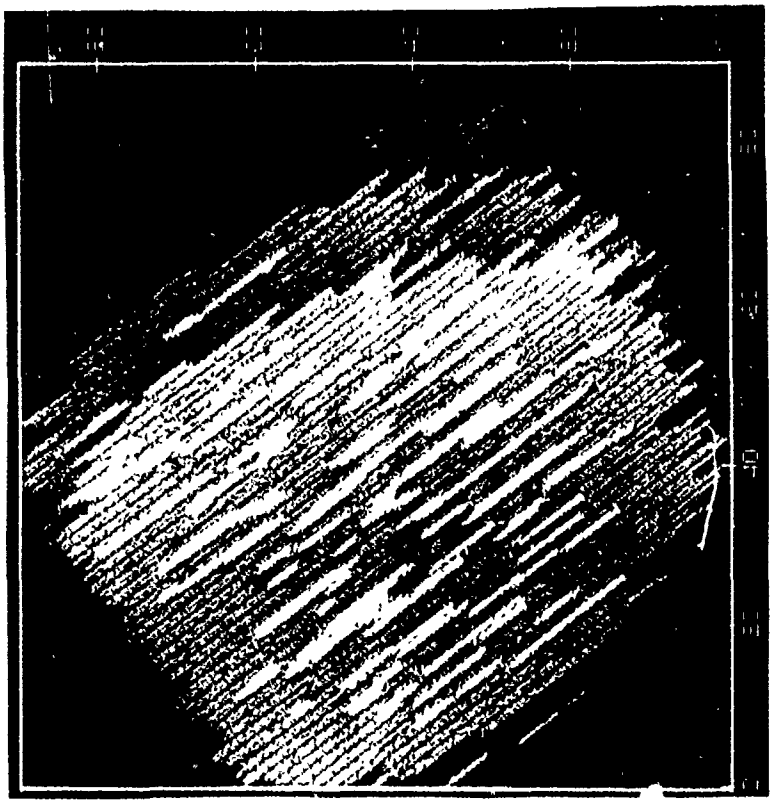

C

FIG 3 (CONTD)

H

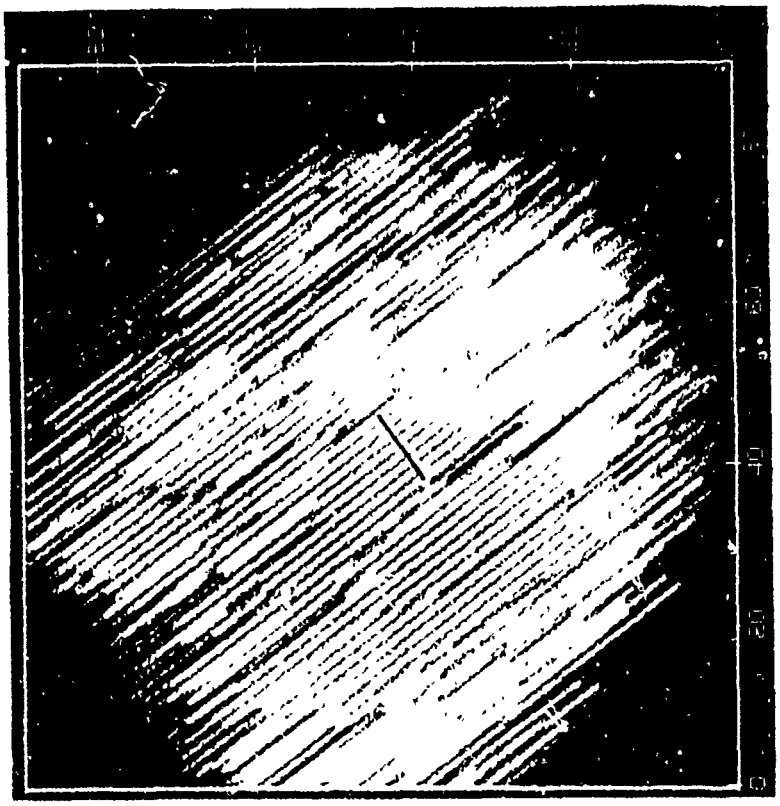

V

FIG 3 (CONTD)

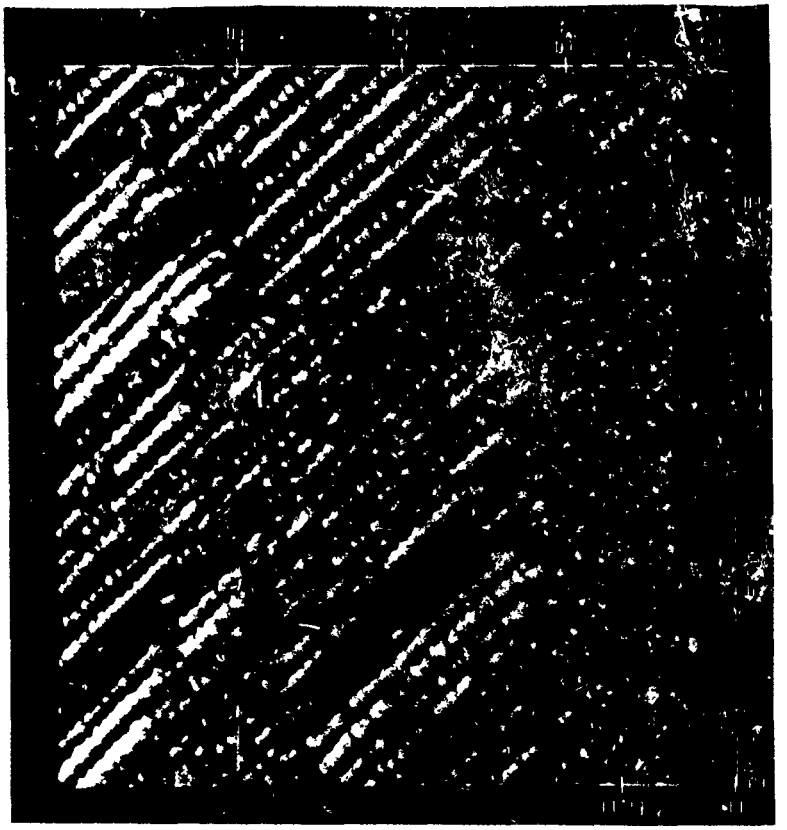

B

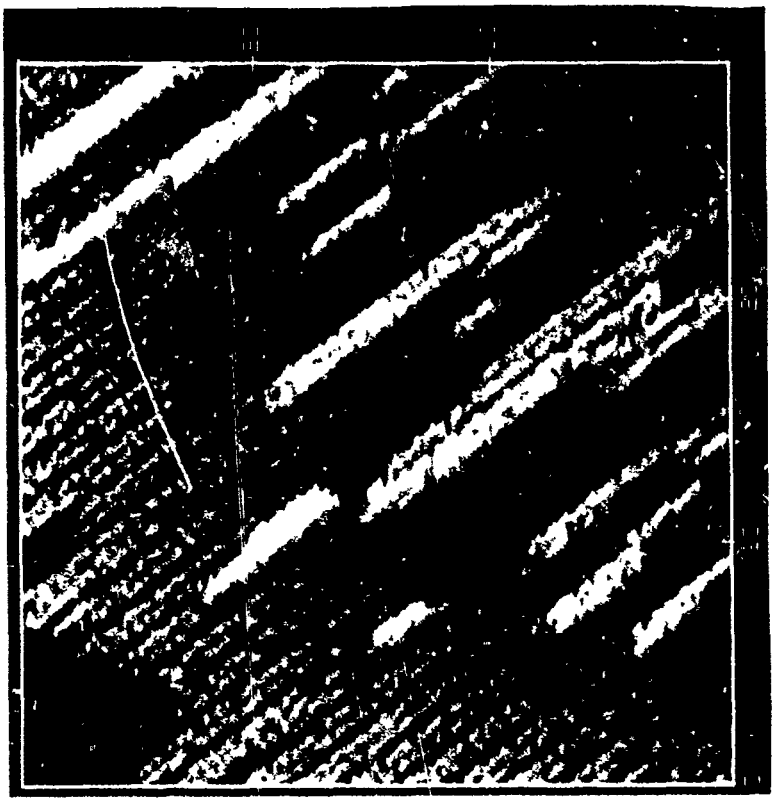

A

FIG 4

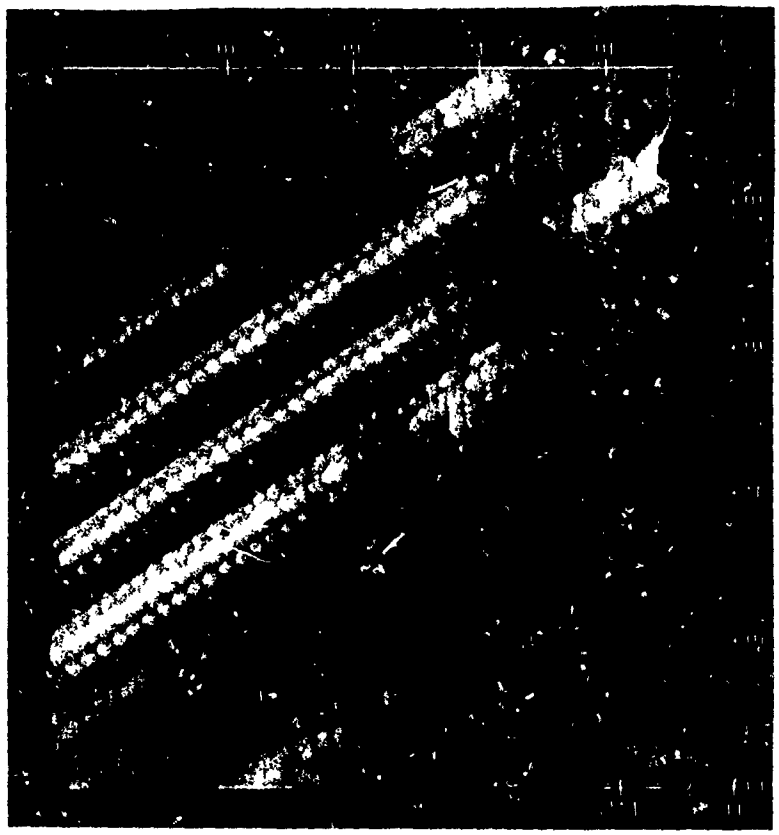

A

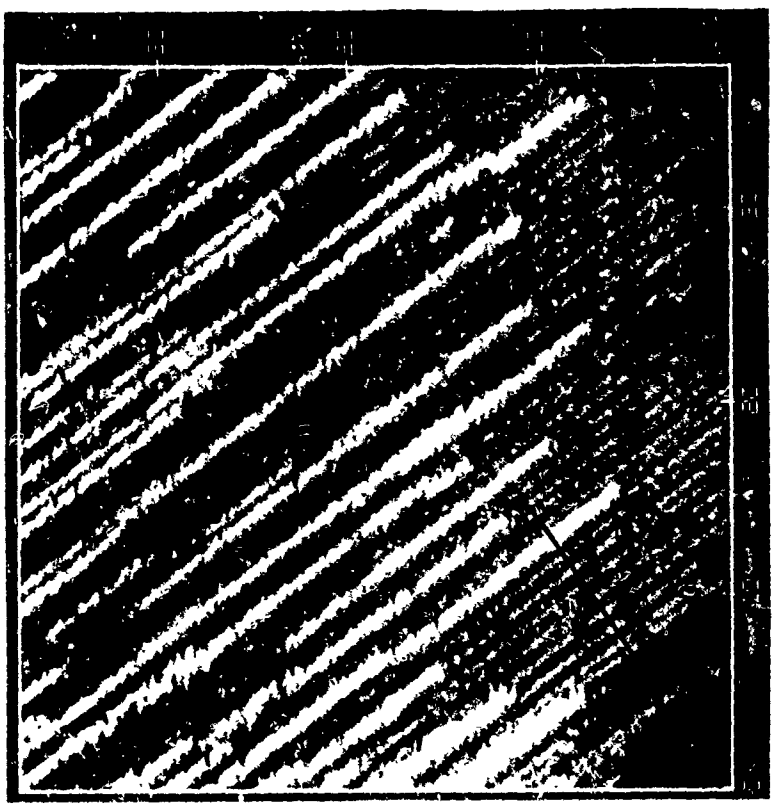

J

FIG 4 (CONTD)

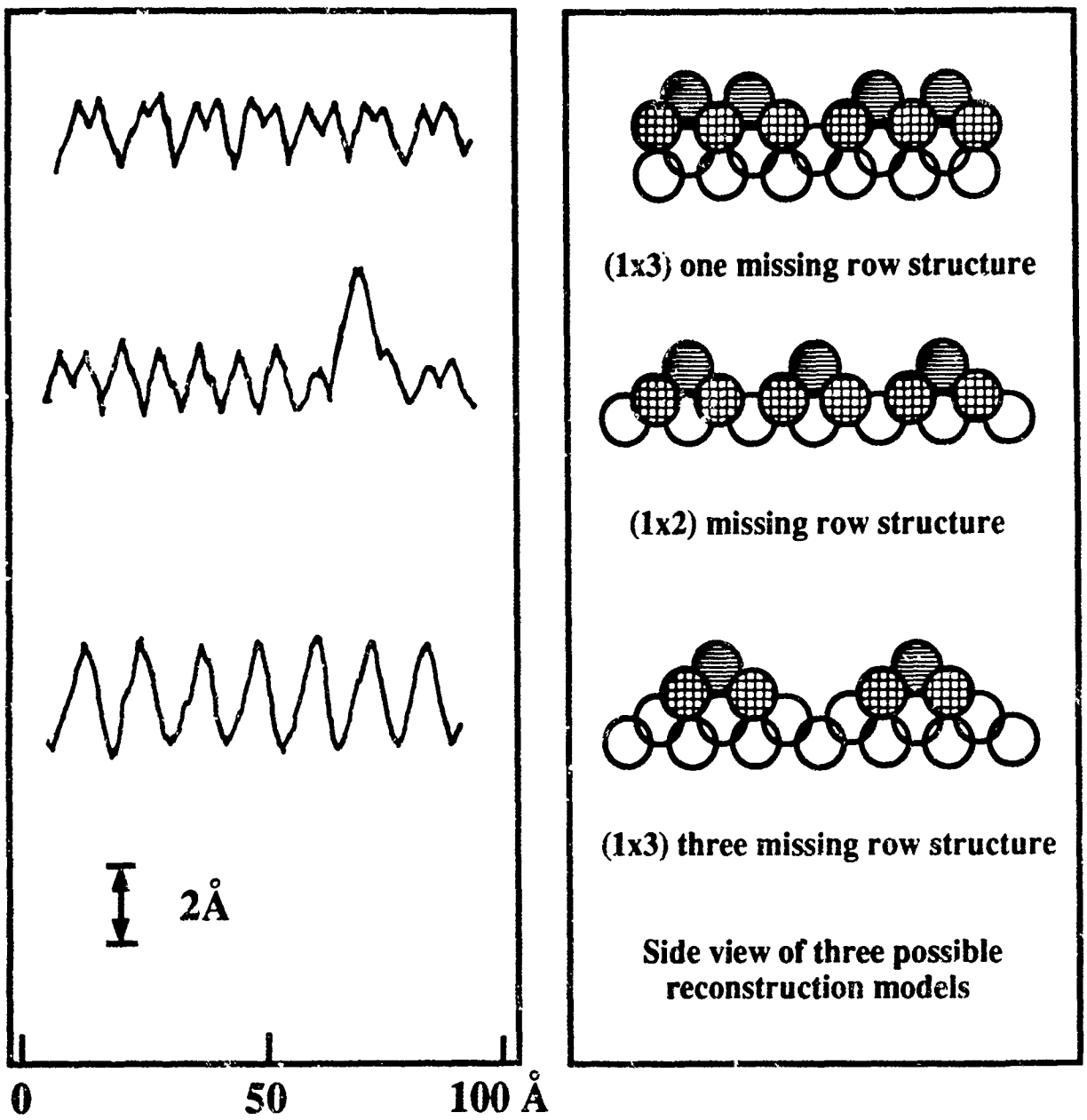
2Å
0
50
100 Å
(1x3) one missing row structure
(1x2) missing row structure
(1x3) three missing row structure
Side view of three possible reconstruction models

FIG 5